

STRUCTURE CHARACTERISTICS OF LIGHT CLUSTER NUCLEI WITH TWO EXTRA NUCLEONS

B.E. GRINYUK, I.V. SIMENOG

PACS 27.20.+n, 21.60.Gx,
21.10.Ft, 21.10.Gv
©2011

Bogolyubov Institute for Theoretical Physics, Nat. Acad. of Sci. of Ukraine
(14b, Metrolohichna Str., Kyiv 03680, Ukraine; e-mail:
bgrinyuk@bitp.kiev.ua, ivsimenog@bitp.kiev.ua)

The cluster nuclei ${}^6\text{Li}$, ${}^6\text{He}$, ${}^{10}\text{Be}$, and ${}^{10}\text{C}$ are studied as systems consisting of α -particles and two extra nucleons. The structure functions of these nuclei are found within the variational approach. The charge density distributions, form factors, and pair correlation functions are presented and explained.

[12]). This approach is known to have a high accuracy for various few-body problems including the problem of near-threshold weakly bound states [13], and it is used successfully even for studying the asymptotics of structure functions of light nuclei [10, 14–17]. In the present paper, we discuss mainly the statement of the problem and physical results obtained, omitting the details of variational calculations.

1. Introduction

In the present paper, we consider some of the light cluster nuclei consisting of an α -cluster and two extra nucleons (they are ${}^6\text{Li}$ and ${}^6\text{He}$ nuclei) or consisting of two α -clusters and two extra nucleons (like the mirror nuclei ${}^{10}\text{Be}$ and ${}^{10}\text{C}$). The α -clusters are usually treated as particles [1–3] or as systems of nucleons [4–7], and these approaches are competitive in accuracy. The main purpose of our consideration is to study the structure functions of the above-mentioned nuclei, especially those connected with the extra nucleons, within the approach [8–10], where the nuclei are considered as consisting of α -particles and two extra nucleons.

To treat the nuclei within such an approach with enough accuracy, one has to deal with the following two problems. The first lies in constructing the $\alpha\alpha$ - and $N\alpha$ -interaction potentials which together with corresponding NN -potentials should provide the description of both the experimental phase shifts at low energies and the main characteristics (binding energy and radius) of the nucleus under consideration. We demonstrate below how this problem is solved. The second one is to calculate the three- and four-body systems with enough accuracy. To study the bound states of nuclear systems, we use well-developed precise calculation procedures based on the variational method with Gaussian bases [11] (see also

2. Statement of the Problem

Consider the six-nucleon nuclei ${}^6\text{Li}$ and ${}^6\text{He}$ within a three-particle model [8, 9] (an α -particle plus two nucleons). The Hamiltonian of ${}^6\text{Li}$ nucleus is used in the form

$$\hat{H} = \frac{\mathbf{p}_p^2}{2m_p} + \frac{\mathbf{p}_n^2}{2m_n} + \frac{\mathbf{p}_\alpha^2}{2m_\alpha} + V_{np}(r_{np}) + \hat{V}_{p\alpha}(r_{p\alpha}) + \hat{V}_{n\alpha}(r_{n\alpha}) + V_C(r_{p\alpha}). \quad (1)$$

The Hamiltonian for ${}^6\text{He}$ nucleus with two halo neutrons has a form similar to (1), but without the Coulomb potential V_C .

Nuclei ${}^{10}\text{Be}$ and ${}^{10}\text{C}$ (in the ground state with $J^\pi = 0^+$), each containing ten nucleons, are considered within a four-particle model [10] (two α -particles plus two nucleons). The four-particle Hamiltonian for ${}^{10}\text{C}$ nucleus differs from (1) mainly by an additional term in the kinetic energy (due to the presence of one more α -particle), an additional interaction potential $\hat{V}_{\alpha\alpha}$ between the α -particles, and by Coulomb interactions between each pair of the charged particles. The Hamiltonian for ${}^{10}\text{Be}$ nucleus is similar to that of ${}^{10}\text{C}$, but with neutrons instead of protons and with only one Coulomb potential

(between the α -particles). We do not indicate these obvious formulae for brevity. It should be noted that we use the Coulomb potential in the form $V_C = Z_1 Z_2 e^2 / r$ valid for charged “point-like” particles, although α -particles and nucleons are known to have a certain charge distribution. This is explained by two reasons. The first lies in a comparatively small contribution of the Coulomb interaction at short distances into the energy and other parameters of the system, thus a modification of this interaction at these distances makes even less contribution. The second one lies in the fact that we have to construct an effective nuclear potential between a pair of particles by fitting its parameters in order to describe the experimental phase shift obtained after the subtraction of the purely Coulomb phase shift. To be consistent, we have to use the obtained nuclear potential together with the same purely Coulomb interaction.

The main problem is to choose the set of interaction potentials in the Hamiltonian in such a way that to describe the main parameters of a nucleus under consideration (such as the energy and the charge radius of the nucleus). Only under such a condition, the model of a nucleus may seem to be realistic. The potentials of interaction between halo nucleons are taken in the form proposed in works [8, 9]. These local spin-dependent potentials allow one to describe the phases of two-nucleon scattering and their low-energy parameters with sufficient accuracy. The np -interaction potential in the triplet state also gives the basic parameters of a deuteron (the experimental binding energy and the charge radius).

The potentials between a nucleon and an α -particle are known to be essentially dependent on the angular momentum, and they should reflect the Pauli principle in the S -state interaction. The scattering phase shift in the S -state should also be equal to π at zero energy [8] in spite of the fact that a nucleon does not form a bound state with an α -particle. All these conditions can be satisfied in a model of $N\alpha$ interaction potential [8, 9] in the form of a superposition of local and non-local operators, which generalizes the model of potentials with forbidden states [2, 18]. We use the simplest version of a non-local operator with one separable term, thus the $N\alpha$ -potential operator has the form:

$$\hat{V}_{N\alpha} \psi(r) = V(r)\psi(r) + gu(r) \int u(r_1)\psi(r_1)d\mathbf{r}_1. \quad (2)$$

For local potentials, one of the simplest methods to calculate the phase shifts and their low-energy parameters is the variable phase approach [19, 20]. But, for non-local potentials, the equations of this method [20] for the phase shifts may contain a function with poles under

the integral at the argument of the exponential function with *a priori* unknown positions of the poles, while the solution itself being free from singularities.

To avoid this problem, we proposed [8, 9] a system of two linear equations for determining the phase shifts without the above-mentioned singularities. Consider the general case of the two particle scattering by a potential of a general form $\hat{V}(\mathbf{r}, \mathbf{r}')$ with additional Coulomb repulsion between particles. The solution $u_l(r)$ of the Schrödinger equation (for an arbitrary partial wave),

$$u_l''(r) + \left(k^2 - \frac{l(l+1)}{r^2} - \frac{2\mu}{\hbar^2} \frac{Z_1 Z_2 e^2}{r} \right) u_l(r) - \int_0^\infty V_l(r, r_1) u_l(r_1) dr_1 = 0, \quad (3)$$

where

$$V_l(r, r_1) = 2\pi r r_1 \int_0^\pi V(\mathbf{r}, \mathbf{r}_1) P_l(\cos \theta) \sin \theta d\theta, \quad (4)$$

can be presented in the form

$$u_l(r) = c_1(r) F_l(kr, \eta) + c_2(r) G_l(kr, \eta). \quad (5)$$

Here, $F_l(kr, \eta)$ and $G_l(kr, \eta)$ are the regular and irregular Coulomb functions, respectively, $\eta \equiv \frac{\mu Z_1 Z_2 e^2}{\hbar^2 k}$ is the Coulomb parameter, μ is the reduced mass of two scattering particles with charges equal to $Z_1 e$ and $Z_2 e$. The system of two linear equations for $c_1(r)$ and $c_2(r)$ can be shown to have the form

$$c_1'(r) = \frac{G_l(kr, \eta)}{k} \int_0^\infty V_l(r, r_1) u_l(r_1) dr_1, \\ c_2'(r) = -\frac{F_l(kr, \eta)}{k} \int_0^\infty V_l(r, r_1) u_l(r_1) dr_1, \quad (6)$$

where $u_l(r_1)$ is expressed through $c_1(r_1)$ and $c_2(r_1)$ according to (5), and the boundary conditions are $c_1(0) \neq 0$ (in particular, $c_1(0) = 1$) and $c_2(0) = 0$. Then the phase shift $\gamma_l(k)$ (which is a part of the total phase shift $\delta_l = \gamma_l + \beta_l$, where β_l is the well-known purely Coulomb phase shift), can be determined from the relation

$$\tan(\gamma_l(k)) = \lim_{r \rightarrow \infty} \frac{c_2(r)}{c_1(r)}. \quad (7)$$

If the Coulomb interaction is absent ($\eta = 0$), then the Coulomb functions in (5), (6) are known [19] to become the Riccati-Bessel functions, $F_l(kr, 0) = j_l(kr)$, and $G_l(kr, 0) = -n_l(kr)$. Since $\beta_l = 0$ in this case, relation (6) gives the total phase shift $\delta_l(k)$. The low-energy parameters of phase shifts can also be determined directly from the corresponding limiting equations. We refer the reader to works [8, 9], where the equations for determining the scattering length are given in an explicit form in both cases of the presence [9] or absence [8] of the Coulomb interaction.

The $\alpha\alpha$ -potentials (necessary for treating the ^{10}Be and ^{10}C nuclei) can also be constructed in the form (2). The known Ali-Bodmer potentials [21] can also be used. We use the both possibilities, and we obtain very close results for these cases.

It should be emphasized that, in order to fix the parameters of potentials to study the structure of a given nucleus, we consider not only the corresponding experimental phase shifts to be described, but also the experimental energy and the charge r.m.s radius of the nucleus under consideration to be explained. Only in this case, the obtained model of a nucleus may give quantitative results [8, 9] for the structure functions of this nucleus. Since phenomenological potentials of simple forms cannot give equally nice results for all the nuclei simultaneously, we adjust the parameters of potentials for each nucleus separately. The parameters of our $N\alpha$ -potentials used for studying ^6He and ^6Li nuclei can be found in [8]. In Table 1, we give the results of our calculations for ^{10}Be nucleus with two following sets of the interaction potentials (intensities – in MeV, radii – in Fm):

$$\hat{V}_{n\alpha} : V(r) = -46.004 \exp(-(r/2.29)^2); \quad g = 140.0/r_0^3,$$

$$u(r) = \pi^{-3/4} \exp(-(r/r_0)^2), \quad r_0 = 2.79,$$

$$\hat{V}_{\alpha\alpha} : V(r) = -47.6 \exp(-(r/2.6)^2) +$$

$$+253.0 \exp(-(r/1.4)^2); \quad g = 60.0/r_0^3,$$

$$u(r) = \pi^{-3/4} \exp(-(r/r_0)^2), \quad r_0 = 1.75, \quad (8)$$

and the second set

$$\hat{V}_{n\alpha} : V(r) = -46.005 \exp(-(r/2.295)^2); \quad g = 140.0/r_0^3,$$

$$u(r) = \pi^{-3/4} \exp(-(r/r_0)^2), \quad r_0 = 2.75,$$

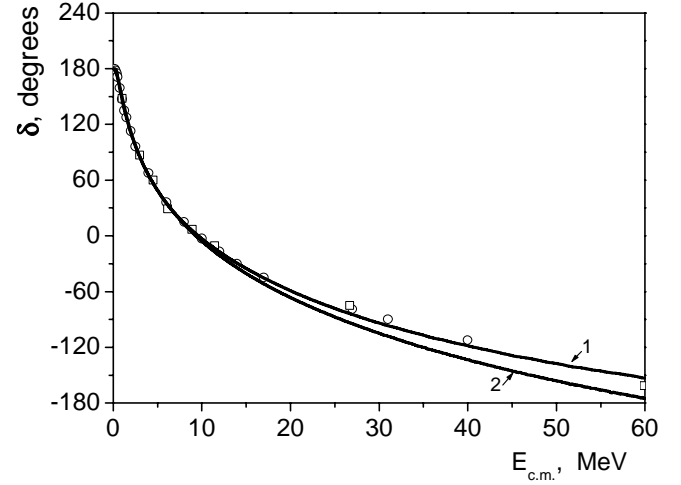


Fig. 1. S -phase shift for the $\alpha\alpha$ -potentials used in our calculations: curve 1 corresponds to our version of potential ($\hat{V}_{\alpha\alpha}$ from (8)), and curve 2 – to the Ali-Bodmer [21] one (see $\hat{V}_{\alpha\alpha}$ in (9)). The circles and squares depict the experimental points

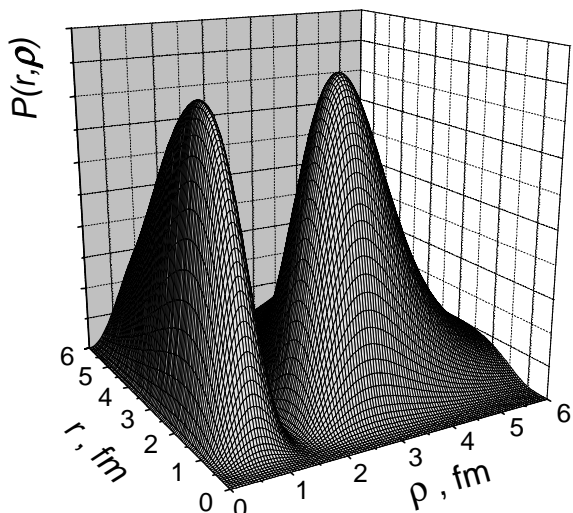
$$\hat{V}_{\alpha\alpha} : V(r) = -130.0 \exp(-(0.475r)^2) + \\ +500.0 \exp(-(0.7r)^2) . \quad (9)$$

The parameters of the potentials $\hat{V}_{n\alpha}$ and $\hat{V}_{\alpha\alpha}$ are fixed to describe the ground state of ^{10}Be . The both sets imply the usage of V_{nn} in the singlet state proposed in [8], otherwise the parameters of potentials should be readjusted a little. The second set of potentials includes one of the versions of Ali-Bodmer potentials [21] for $\alpha\alpha$ -interaction in the S -state. Since the contribution of the $\alpha\alpha$ -interaction in nonzero partial states into the ground state of ^{10}Be is negligible, we ignore the l -dependence of the Ali-Bodmer potential in our calculations. It should be noted that the both sets of potentials give almost the same values for all the main parameters of ^{10}Be nucleus (see Table 1) and its structure functions (they almost coincide in the figures). Note also that the both versions of $\alpha\alpha$ -potentials do not bind a system of two α -particles and give a reasonable description of the S -phase shift of the $\alpha\alpha$ scattering at low energies (see Fig. 1).

The solution of the three- and four-body problems is carried out [8–10, 14, 15] in the framework of the variational method in the Gaussian representation [11, 12]. We omit the details of this well-known method. We only note that a high accuracy of calculations was achieved, by using about 200 to 300 functions of the optimized Gaussian basis. One more important remark concerns with the fact that, within the variational calculations

Table 1. Calculated energy (MeV) and root-mean-square radii (Fm) for ^{10}Be nucleus

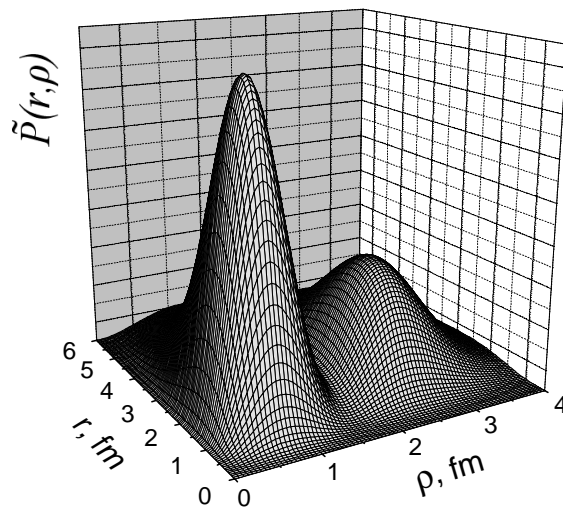
Set of potentials $\hat{V}_{n\alpha}, \hat{V}_{\alpha\alpha}$	$E(^{10}\text{Be})$	$R_{\text{ch}}(^{10}\text{Be})$	r_{nn}	$r_{n\alpha}$	$r_{\alpha\alpha}$	R_n	R_α
$\hat{V}_{n\alpha}, \hat{V}_{\alpha\alpha}$: (8)	-8.387	2.357	3.074	2.850	3.230	2.091	1.654
$\hat{V}_{n\alpha}, \hat{V}_{\alpha\alpha}$: (9)	-8.387	2.357	3.080	2.859	3.229	2.100	1.654
Experiment	-8.3867	2.357(21)					

Fig. 2. Probability density distribution $P(r, \rho)$ (10) for a halo neutron in ^6He nucleus

with Gaussian bases, while the calculated energy of the system converges to the exact value monotonically from above, the rest values (like r.m.s. radii) converge to their limiting values without such a regularity, and their precision may be a little bit less than that of the energy.

3. General Structure of Three- and Four-Cluster Nuclei with Two Extra Nucleons

The main properties of the structure functions of ^6He and ^6Li nuclei are explained within a three-particle model by the presence of two configurations in their wave functions (the “triangle” and “cigar” configurations [1–3, 8, 9]). The variational method with Gaussian bases [11, 12] enables us to obtain the wave functions of ^6He and ^6Li nuclei with high accuracy [8, 9] in an explicit form of a superposition of Gaussian functions suitable for the further usage and analysis. Let $\Phi(\mathbf{r}, \boldsymbol{\rho})$ denote the wave function of ^6Li nucleus in a three-particle model (\mathbf{r} is the relative coordinate between the halo nucleons, and $\boldsymbol{\rho}$ is the coordinate of an α -particle with respect to the center of mass of the halo nucleons). In Fig. 2, the

Fig. 3. Calculated probability density $\tilde{P}(r, \rho)$ (11) for ^{10}C nucleus

probability density

$$P(r, \rho) = r^2 \rho^2 \left\langle |\Phi(\mathbf{r}, \boldsymbol{\rho})|^2 \right\rangle_{\Omega} \quad (10)$$

(with an averaging over the angles) is shown for ^6He nucleus. A similar picture can be drawn for ^6Li nucleus. The general properties of the structure of these probability densities is discussed in detail in [8, 9].

In the case of four-particle nuclei ^{10}Be and ^{10}C , we have one more Jacobi coordinate variable in the four-particle wave function $\Phi(\mathbf{r}, \boldsymbol{\rho}, \mathbf{r}_{\alpha\alpha})$, where $r_{\alpha\alpha}$ is the relative distance between α -clusters, and $\boldsymbol{\rho}$ is the distance between the center of mass of two α -clusters and the center of mass of the pair of extra nucleons. The distance between the extra nucleons is again denoted by r . To depict the probability density for the extra nucleons, we have to reduce the number of variables. In Fig. 3, the quantity

$$\tilde{P}(r, \rho) = r^2 \rho^2 \left\langle \int |\Phi(\mathbf{r}, \boldsymbol{\rho}, \mathbf{r}_{\alpha\alpha})|^2 d\mathbf{r}_{\alpha\alpha} \right\rangle_{\Omega} \quad (11)$$

with an additional integration over the relative coordinate between the two α -particles is shown for ^{10}C nucleus. Like in Fig. 2, again two peaks are clearly seen in the probability density for two extra nucleons. But now they come from a “tetrahedron” configuration (instead of a “triangle” one) in ^6He and ^6Li nuclei, where

two extra nucleons form a two-particle cluster moving around the center of mass of the nucleus together with the $\alpha\alpha$ -cluster, and a “cross” configuration (instead of a “cigar” one) in a three-particle nucleus), where extra nucleons are at the opposite sides from the $\alpha - \alpha$ axis. Very similarly to Fig. 3, a picture can be drawn for ^{10}Be nucleus (see [10]). It should be noted that probability distributions calculated for α -particles in ^{10}Be and ^{10}C nuclei (with the integration of the squared wave function over the relative coordinate of two extra nucleons) also distinctly show two peaks.

The specific configurations present in the wave functions reveal themselves in all the structure functions of the nuclei.

4. One-Particle Density Distributions, Form Factors, and Pair Correlation Functions

The probability density for the i -th particle in a system of particles with the wave function $|\Phi\rangle$ is known to be

$$n_i(r) = \langle \Phi | \delta(\mathbf{r} - (\mathbf{r}_i - \mathbf{R}_{c.m.})) | \Phi \rangle, \quad (12)$$

where $\mathbf{R}_{c.m.}$ denotes the center of mass of the system. Here and further, the density distributions are normalized as $\int n_i(r) d\mathbf{r} = 1$.

The r.m.s. radius R_i of this distribution,

$$R_i = \langle r_i^2 \rangle^{1/2} = \left(\int r^2 n_i(r) d\mathbf{r} \right)^{1/2}, \quad (13)$$

determines the slope of the corresponding form factor (the Fourier transformation $F_i(q^2)$ of $n_i(r)$) at small transferred momenta,

$$F_i(q^2) = 1 - \frac{1}{6} \langle r_i^2 \rangle q^2 + \dots = \sum_{k=0}^{\infty} \frac{(-1)^k}{(2k+1)!} \langle r_i^{2k} \rangle q^{2k}. \quad (14)$$

Consider the density distributions for “point-like” particles, of which the examined nuclei are composed in the three-particle model.

First, let us consider the distribution of α -particles. In Fig. 4, we compare $r^2 n_\alpha(r)$ (the probability density with regard for $\sim r^2$) calculated for ^6Li nucleus containing one α -particle with that for ^{10}Be nucleus having two α -particles. Note that the density distribution $n_\alpha(r)$ for ^6He nucleus is similar, to a great extent, to that for ^6Li (see [8, 9]), and $n_\alpha(r)$ calculated for ^{10}C is similar to that for ^{10}Be . That is why we show only two curves in Fig. 4, one for the case of a

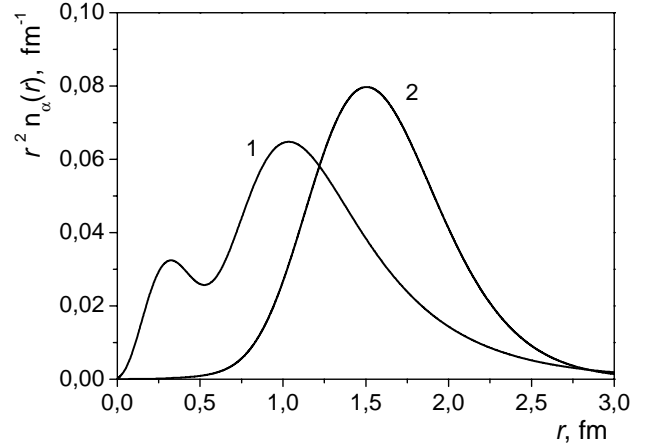


Fig. 4. Calculated α -particle density distributions (multiplied by r^2) for ^6Li (curve 1) and for ^{10}C (curve 2) nuclei

three-cluster nucleus (with one α -particle), and the second – for the case of a four-cluster one (with two α -particles). Two peaks of the α -particle distribution for ^6Li nucleus are explained by the presence of two different configurations mentioned above in the total wave function: the peak near the origin is present due to the “cigar” configuration, where the α -particle moves near the center of mass of the nucleus, while the second peak comes from the “triangle” configuration, where the α -particle and the deuteron cluster move around the common center of mass at a definite distance from it. As to ^{10}Be nucleus, its both configurations contain the ^8Be cluster, where two α -particles are at a definite distance each from other, and the center of mass of the ^8Be cluster is not far from the center of mass of ^{10}Be nucleus. That is why the curve 2 in Fig. 4 has one peak.

The probability densities of extra nucleons in the three- and four cluster nuclei under consideration are depicted in Fig. 5 (the distribution of the halo proton in ^6Li is very close to the distribution of the neutron shown in Fig. 5, but has a little bit greater radius [9]). Since the extra nucleons in ^{10}Be and ^{10}C nuclei are present mainly in the “cross” configuration, where ρ is comparatively small (see Fig. 3), while in ^6He and ^6Li nuclei, *vice versa*, in the “triangle” configuration, where ρ is larger (see Fig. 2), the halo nucleons in ^6He and ^6Li nuclei are seen (Fig. 5) to move at greater average distances than the extra nucleons in ^{10}Be and ^{10}C nuclei. The contrary situation with the α -particle density distributions in these nuclei (see Fig. 4) leads to the presence of a pronounced halo in the three-cluster nuclei ^6He and ^6Li

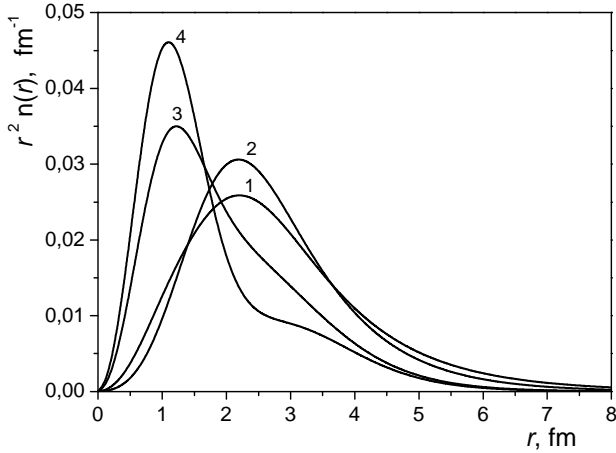


Fig. 5. Calculated halo neutron density distributions (multiplied by r^2) for ${}^6\text{He}$ (curve 1) and for ${}^6\text{Li}$ (curve 2) nuclei. The calculated density distributions for the extra proton of ${}^{10}\text{C}$ (curve 3) and for the extra neutron of ${}^{10}\text{Be}$ (curve 4)

moving around the α -particle, while the extra nucleons in the four-cluster nuclei ${}^{10}\text{Be}$ and ${}^{10}\text{C}$ are moving almost inside their nuclei due to the presence of a cluster of ${}^8\text{Be}$ comparable in size. We note also that the asymptotics of the density distributions of halo nucleons were studied for ${}^6\text{He}$ and ${}^6\text{Li}$ nuclei in [14, 15] in detail. Although the structure of ${}^6\text{He}$ nucleus is, from the qualitative point of view, similar to that of ${}^6\text{Li}$ at distances within a few Fm, the asymptotic behaviors of the density distributions of these nuclei are essentially different [14, 15]. This is explained by the fact that ${}^6\text{He}$ has a three-particle breakup threshold (${}^6\text{He} \rightarrow n + n + \alpha$), while ${}^6\text{Li}$ has the two-particle one (${}^6\text{Li} \rightarrow d + \alpha$), and this nucleus is rather weakly bound. Therefore, the wave function of ${}^6\text{He}$ (within a three-particle model) has a three-particle Merkuriev asymptotics [22, 23], whereas the wave function of ${}^6\text{Li}$ has the two-particle one (formed by the short-range potentials and the Coulomb repulsion). Explicit formulae [14, 15] obtained for the asymptotics of the density distributions of ${}^6\text{He}$ and ${}^6\text{Li}$ nuclei are confirmed by numerical calculations within the variational method with the Gaussian bases up to the distances, where the density distributions become 10^{-9} as compared with the maximum value.

To calculate the charge density distribution $n_{\text{ch}}(r)$ of a nucleus, we have to consider the charge distribution of the α -particle itself, as well as the charge distribution of the extra proton (for simplicity, we neglect the charge distribution of the extra neutron). If the nucleus contains N_α of α -particles and N_p of protons, then, in the Helm approximation [24], the charge distribution of the

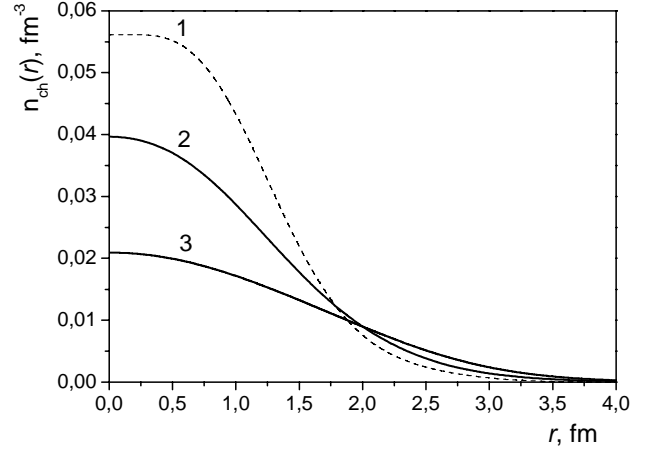


Fig. 6. Charge density distribution for ${}^4\text{He}$ [25] (curve 1) and calculated distributions for ${}^6\text{He}$ (curve 2) and ${}^{10}\text{Be}$ (curve 3) nuclei. All the distributions are normalized to 1

nucleus (normalized to 1) reads

$$n_{\text{ch}}(r) = \frac{2N_\alpha}{2N_\alpha + N_p} \int n_\alpha(|\mathbf{r} - \mathbf{r}_1|) n_{\text{ch},{}^4\text{He}}(r_1) d\mathbf{r}_1 + \frac{N_p}{2N_\alpha + N_p} \int n_p(|\mathbf{r} - \mathbf{r}_1|) n_{\text{ch},p}(r_1) d\mathbf{r}_1, \quad (15)$$

where the one-particle density distributions $n_\alpha(r)$ and $n_p(r)$ are calculated according to (12), $n_{\text{ch},{}^4\text{He}}(r)$ is the charge distribution of the α -particle [25] itself, and $n_{\text{ch},p}(r)$ is that of the proton [26].

In Fig. 6, the charge density distributions (normalized to 1) are shown for ${}^4\text{He}$ (i.e. “free” α -particle, curve 1, from [25]), for ${}^6\text{He}$ (where an α -particle is moving around the center of mass of the nucleus together with two halo neutrons, curve 2), and ${}^{10}\text{Be}$ (where two α -particles are combined in a ${}^8\text{Be}$ cluster surrounded by two extra neutrons, curve 3).

Consider the charge form factors which are the Fourier transforms of the charge density distributions. Starting from (15), one has

$$F_{\text{ch}}(q) = \frac{2N_\alpha}{2N_\alpha + N_p} F_\alpha(q) F_{\text{ch},{}^4\text{He}}(q) + \frac{N_p}{2N_\alpha + N_p} F_p(q) f_p(q), \quad (16)$$

where $F_\alpha(q) = \int e^{-i(\mathbf{q}\mathbf{r})} n_\alpha(r) d\mathbf{r}$ is the form factor of a “point-like” α -particle in the nucleus under consideration, $F_{\text{ch},{}^4\text{He}}(q)$ is the charge form factor of an α -particle (i.e. of ${}^4\text{He}$ nucleus), $F_p(q) = \int e^{-i(\mathbf{q}\mathbf{r})} n_p(r) d\mathbf{r}$ is the

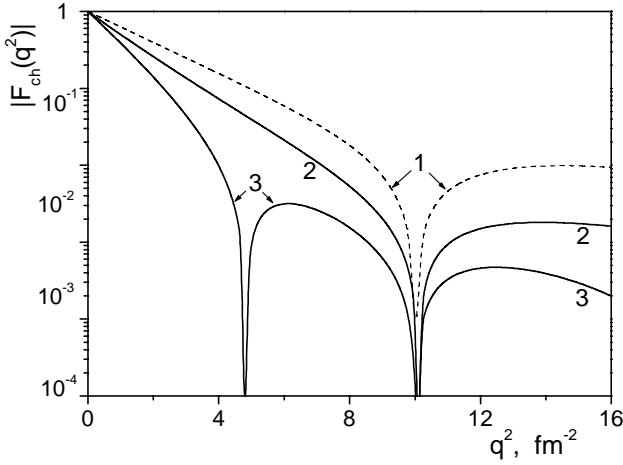


Fig. 7. Experimental charge form factor for ${}^4\text{He}$ [25] (curve 1) and calculated charge form factors for ${}^6\text{He}$ (curve 2) and ${}^{10}\text{Be}$ (curve 3) nuclei

form factor of a “point-like” extra proton of this nucleus, and $f_p(q)$ is the charge form factor of the proton itself. We neglect the contribution of the charge form factor of a neutron. In Fig. 7, we compare the charge form factors of the nuclei ${}^4\text{He}$, ${}^6\text{He}$, and ${}^{10}\text{Be}$, where the charge distributions are explained mainly by the presence of charged α -particles. The presence of the “dip” in the charge form factors of ${}^6\text{He}$ and ${}^{10}\text{Be}$ nuclei at $q^2 \sim 10 \text{ Fm}^{-2}$ is directly related to the characteristic feature of the experimental form factor of ${}^4\text{He}$ having such a “dip”, because only the first term in (16) contributes to the charge form factors of these nuclei, and thus they are proportional to the ${}^4\text{He}$ form factor. The first “dip” in the form factor of ${}^{10}\text{Be}$ at $q^2 \sim 5 \text{ Fm}^{-2}$ is an evidence of the presence of the ${}^8\text{Be}$ cluster in ${}^{10}\text{Be}$ nucleus, which results in specific properties of $n_\alpha(r)$ (see Figs. 4 and 9) and in its Fourier transform $F_\alpha(q)$ in the case of ${}^{10}\text{Be}$.

The charge form factor of ${}^{10}\text{C}$ nucleus differs from that of ${}^{10}\text{Be}$ one, because the second term in (16) is nonzero due to the presence of extra protons. As a result, the charge form factor of ${}^{10}\text{C}$ has no “dips” within the region of q^2 shown in Fig. 7 since $F_{\text{ch}}(q)$ (16) for this nucleus approaches zero neither at $q^2 \sim 10 \text{ Fm}^{-2}$, where $F_{\text{ch},{}^4\text{He}}(q) = 0$, nor at $q^2 \sim 5 \text{ Fm}^{-2}$, where $F_\alpha(q) = 0$. For the charge form factor of ${}^{10}\text{C}$ nucleus, the first “dip” appears after $q^2 \sim 18 \text{ Fm}^{-2}$.

Consider the problem of determining the r.m.s. radius from an experimental form factor at low transferred momenta. Consider, for example, the charge form factor of ${}^6\text{Li}$ nucleus. As clearly seen from Fig. 8, it is almost impossible to determine the coefficients of expansion (14) by directly using this series, because the first two terms

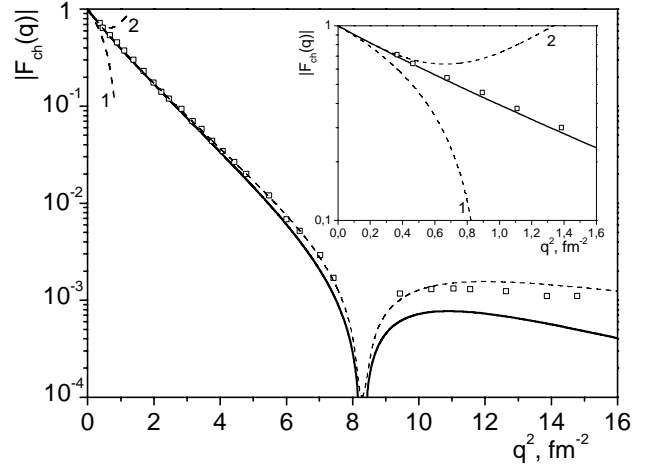


Fig. 8. Calculated charge form factor for ${}^6\text{Li}$ (solid line). Squares are the experimental values. Curve 1 (in the figure and in the insert) shows the two-term approximation (14) for the form factor, and curve 2 shows the three-term one. The dashed line (close to experimental points) depicts our representation (17) for the form factor

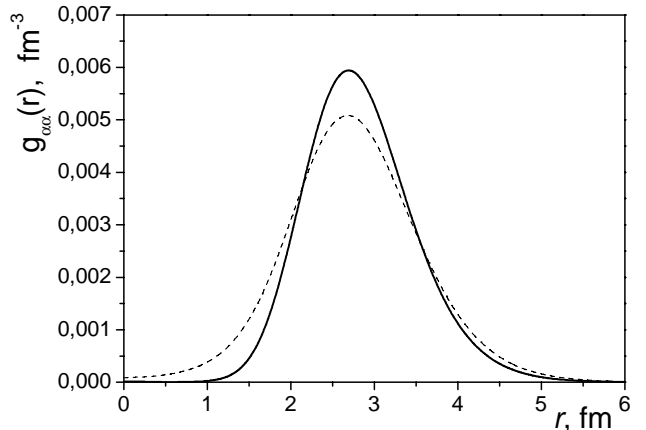


Fig. 9. Two- α -particle correlation function for ${}^{10}\text{Be}$ nucleus (solid curve). The dashed line depicts $\frac{1}{8}n_\alpha(\frac{r}{2})$

of (14) (curve 1) or even three terms (curve 2) can serve to be an approximation for a form factor only at extremely small q^2 . This produces obvious difficulties for the determination of the r.m.s. radius with high accuracy from the slope of the experimental form factor.

We proposed [14, 15] to expand the inverse form factor with explicitly excluded factors responsible for the “dips”. In particular,

$$F_{\text{ch},{}^6\text{Li}}(q) \cong \frac{1 - \frac{q^2}{q_{\text{min}}^2}}{1 + S_2q^2 + S_4q^4 + S_6q^6 + S_8q^8 + \dots}, \quad (17)$$

where

$$\begin{aligned}
 S_2 &\equiv \frac{\langle r^2 \rangle_{\text{ch}}}{6} - \frac{1}{q_{\text{min}}^2}, & S_4 &\equiv \frac{\langle r^2 \rangle_{\text{ch}}}{6} S_2 - \frac{\langle r^4 \rangle_{\text{ch}}}{120}, \\
 S_6 &\equiv \frac{\langle r^6 \rangle_{\text{ch}}}{7!} + 2S_2 S_4 - S_2^3 + (S_4 - S_2^2) \frac{1}{q_{\text{min}}^2}, \\
 S_8 &\equiv S_2^4 + S_4^2 + 2S_2 S_6 - 3S_2^2 S_4 + \\
 &+ (S_2^3 + S_6 - 2S_2 S_4) \frac{1}{q_{\text{min}}^2} - \frac{\langle r^8 \rangle_{\text{ch}}}{9!}. \quad (18)
 \end{aligned}$$

In expansion (17), we use the experimental values $q_{\text{min}}^2 \approx 8.3 \text{ Fm}^{-2}$ and $\langle r^2 \rangle_{\text{ch}}^{1/2} \equiv R_{\text{ch}} = 2.56 \text{ Fm}$ [27]. The rest parameters, $\langle r^4 \rangle_{\text{ch}}^{1/4} = 3.19 \text{ Fm}$, $S_6 = 0.07 \text{ Fm}^6$, and $S_8 = 0.006 \text{ Fm}^8$ were fitted to reproduce the experimental data (compare the dashed line in Fig. 8 with the experiment). It is interesting that all the parameters S_{2k} appeared to be positive and decreasing with increase in their number. Note that only three free parameters in representation (17) enable one to fit a form factor at small and intermediate transferred momenta including the ‘‘dip’’ region. Thus, representation (17) is much more adequate and suitable than the commonly used expansion (14) in order to analyze the slope of a form factor and to determine the r.m.s. radius from the experimental data (and to find even such parameters as $\langle r^4 \rangle_{\text{ch}}^{1/4}$).

Consider the pair correlation functions of particles constituting the nuclei. The pair correlation function $g_{ij}(r)$ is determined as

$$g_{ij}(r) = \langle \Phi | \delta(\mathbf{r} - (\mathbf{r}_i - \mathbf{r}_j)) | \Phi \rangle, \quad (19)$$

and it is a probability density to find the pair of particles i and j of the system under consideration at a distance r . For local pair potentials, the average potential energy is directly expressed in terms of the integrals over the potentials multiplied by the corresponding correlation functions. The r.m.s. relative distances between a pair of particles i and j is expressed through the pair correlation function as

$$r_{ij} \equiv \left\langle (\mathbf{r}_i - \mathbf{r}_j)^2 \right\rangle^{1/2} = \left(\int r^2 g_{ij}(r) dr \right)^{1/2}. \quad (20)$$

We give also the identities which express the r.m.s. radii R_i through the r.m.s. relative distances r_{ij} . For a three-particle system, one has

$$R_i^2 = a_{jk} r_{ij}^2 + a_{kj} r_{ik}^2 - b_i r_{jk}^2,$$

$$(i, j, k) = (1, 2, 3), \quad i \neq j \neq k,$$

$$a_{jk} \equiv \frac{m_j(m_j + m_k)}{(m_1 + m_2 + m_3)^2}, \quad b_i \equiv \frac{m_j m_k}{(m_1 + m_2 + m_3)^2}, \quad (21)$$

and, for a four-particle system,

$$R_i^2 = \gamma_j r_{ij}^2 + \gamma_k r_{ik}^2 + \gamma_n r_{in}^2 - \beta_{jk} r_{jk}^2 - \beta_{jn} r_{jn}^2 - \beta_{kn} r_{kn}^2,$$

$$(i, j, k, n) = (1, 2, 3, 4), \quad i \neq j \neq k \neq n,$$

$$\gamma_j \equiv \frac{m_j(m_j + m_k + m_n)}{(m_1 + m_2 + m_3 + m_4)^2},$$

$$\beta_{jk} \equiv \frac{m_j m_k}{(m_1 + m_2 + m_3 + m_4)^2}. \quad (22)$$

In (21) and (22), m_i denotes the mass of particle i . Identities (21) and (22) can be used for finding the r.m.s. radii R_i after the r_{ij} are calculated or to verify the results of independent calculations of R_i and r_{ij} .

For three-cluster nuclei ${}^6\text{He}$ and ${}^6\text{Li}$, a detailed analysis of the pair correlation functions is carried out in [8, 9, 14, 15]. Here, we consider $g_{ij}(r)$ for ${}^{10}\text{Be}$ and ${}^{10}\text{C}$ nuclei within our four-particle model. In Fig. 9, the two- α -particle correlation function $g_{\alpha\alpha}(r)$ is shown for ${}^{10}\text{Be}$ nucleus. The pair correlation function has a pronounced maximum at a distance of $\sim 3 \text{ Fm}$, and it is almost zero at short distances. This means that the comparatively heavy α -particles are positioned mainly near the minimum of the $\alpha\alpha$ -potential well, and they do not penetrate into each other due to the Pauli principle which is simulated by a strong repulsion in the $\alpha\alpha$ -interaction potential. If it were simply the two-particle bound system (without additional extra neutrons), then the one-particle density distribution $n_\alpha(r)$ renormalized as $\frac{1}{8}n_\alpha(\frac{r}{2})$ should exactly coincide with the pair correlation function $g_{\alpha\alpha}(r)$ (this fact obviously follows from definitions (12) and (19)). But comparatively light two extra neutrons present in ${}^{10}\text{Be}$ break this coincidence, and only the qualitative agreement is observed (see the dashed line in Fig. 9). Note that the correlation function $g_{\alpha\alpha}(r)$ for ${}^{10}\text{C}$ nucleus is very close to that of ${}^{10}\text{Be}$. This means that the ${}^8\text{Be}$ cluster in the both nuclei has practically the same structure.

Consider the correlation function $g_{nn}(r)$ calculated for ${}^6\text{He}$ and ${}^{10}\text{Be}$ nuclei. The nn -interaction potential used for both nuclei is the same [8]. That is why the profiles of $g_{nn}(r)$ for the both nuclei (see Fig. 10, curves 1

and 3) are very similar at short distances. They differ in the absolute magnitude mainly due to their different r.m.s. relative distances ($r_{nn} \cong 3.08$ Fm for ^{10}Be and $r_{nn} \cong 4.39$ Fm for ^6He), which results, under the normalization condition $\int g(r) dr = 1$, in the corresponding values of $g_{nn}(r)$ near the origin. In the same figure, we depict also the correlation function $g_{pp}(r)$ between the protons in the ^{10}C nucleus (curve 2). For simplicity, we used the same nuclear potential for the pp -interaction in the singlet state as that for the nn -interaction. As is seen from the figure, the Coulomb repulsion between the protons makes almost no influence on the profile of $g_{pp}(r)$ at short distances. Having the r.m.s. relative distance $r_{pp} \cong 3.41$ Fm, the function $g_{pp}(r)$ occupies a position between the rest two curves.

5. Moments of Inertia for ^{10}Be and ^{10}C Nuclei

For spherical nuclei, the inertia tensor becomes a diagonal one, and we deal with the moment of inertia

$$I_z = m \int (x^2 + y^2) n(r) dr = \frac{2}{3} m \int r^2 n(r) dr = \frac{2}{3} m R_m^2, \quad (23)$$

where R_m is the r.m.s. matter radius of the nucleus. Since the r.m.s. radii for the ground states are calculated, we immediately have the calculated moments of inertia for nuclei ^{10}Be and ^{10}C in the ground state (see Table 2 for the set of potentials (9)).

The shifts of energies of a rotational band of a spherical nucleus are known to be

$$\Delta E_J = \frac{\hbar^2 J(J+1)}{2I_z}. \quad (24)$$

We compare the estimations of ΔE_J obtained with the use of (24) and the experimental values [28]. It is clear from Table 2 that the first excited state of nucleus ^{10}Be or ^{10}C (with $J^\pi = 2^+$) can be supposed to be a rotational state of this nucleus almost without deformation of its ground state (since I_z is calculated for the ground state). The agreement of the estimated energy shift $\Delta E = 11.4$

Table 2. Calculated moments of inertia and ΔE_J (for $J^\pi = 2^+$)

Nucleus	I_z/\hbar^2 , MeV $^{-1}$	ΔE_J , MeV	$\Delta E_{J, \text{exper}}$, MeV
^{10}Be	0.876	3.426	3.368
^{10}C	0.934	3.212	3.354

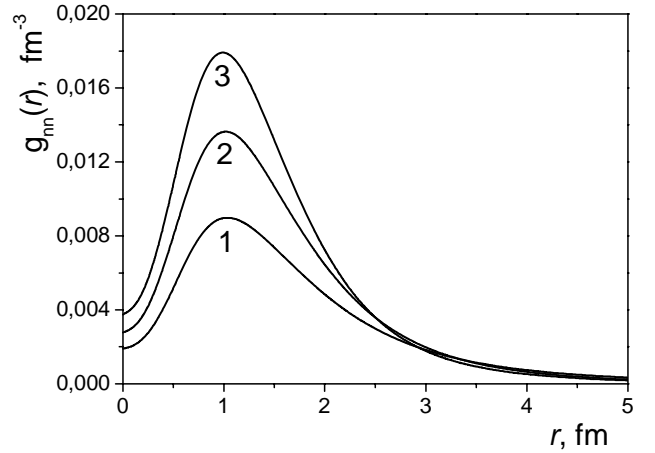


Fig. 10. Calculated pair correlation function $g_{mn}(r)$ for ^6He (curve 1) and ^{10}Be (curve 3) nuclei. Curve 2 depicts the correlation function $g_{pp}(r)$ for ^{10}C nucleus

MeV for the $J^\pi = 4^+$ state of ^{10}Be with the experimental value $\Delta E_{\text{exper}} = 11.76$ MeV is also observed. This enables us to suppose that the $J^\pi = 4^+$ state of ^{10}C with the estimated energy shift $\Delta E = 10.7$ MeV may exist. The experiment [28] shows the existence of an energy level with $\Delta E \approx 10$ MeV with the unknown angular momentum for ^{10}C nucleus.

6. Conclusions

To summarize, we note that the light cluster nuclei ^6Li , ^6He , ^{10}Be , and ^{10}C are treated as those consisting of α -particles and two extra nucleons. Potentials of $N\alpha$ - and $\alpha\alpha$ -interaction are proposed, and the ground states of three- and four-particle nuclei are studied using the variational calculations with Gaussian bases. The main structure functions of the above nuclei are found. The charge density distributions are calculated and explained. The charge form factor of ^6Li nucleus is explained, and those of ^6He , ^{10}Be , and ^{10}C nuclei are predicted. A new suitable representation of form factors at small and intermediate transferred momenta is proposed. The rotational band levels of ^{10}Be and ^{10}C nuclei are estimated.

1. M.V. Zhukov, B.V. Danilin, D.V. Fedorov *et al.*, Phys. Rep. **231**, 151 (1993).
2. V.I. Kukulin, V.N. Pomerantsev, Kh.D. Razikov *et al.*, Nucl. Phys. **A 586**, 151 (1995).
3. E. Nielsen, D.V. Fedorov, A.S. Jensen, and E. Garrido, Phys. Rep. **347**, 373 (2001).
4. V.S. Vasilevsky, A.V. Nesterov, F. Arickx, and P. Van Leuven, Yad. Fiz. **60**, 412 (1997).

5. A.V. Nesterov, F. Arickx, J. Broeckhove, V.S. Vasilevsky, EChAYa **41**, 1337 (2010).
6. K. Varga and Y. Suzuki, Phys. Rev. C **52**, 2885 (1995).
7. Y. Ogawa, K. Arai, Y. Suzuki, and K. Varga, Nucl. Phys. A **673**, 122 (2000).
8. B.E. Grinyuk and I.V. Simenog, Yad. Fiz. **72**, 10 (2009).
9. B.E. Grinyuk and I.V. Simenog, Yad. Fiz. Energ. **10**, 9 (2009).
10. B.E. Grinyuk and I.V. Simenog, Yad. Fiz. Energ. **12**, 1 (2011).
11. V.I. Kukulín and V.M. Krasnopol'sky, J. Phys. G **3**, 795 (1977).
12. Y. Suzuki and K. Varga, *Stochastic Variational Approach to Quantum-Mechanical Few-Body Problems* (Springer, Berlin, 1998).
13. I.V. Simenog, Yu.M. Bidasyuk, B.E. Grinyuk, and M.V. Kuzmenko, Ukr. J. Phys. **52**, 77 (2007).
14. B.E. Grinyuk and I.V. Simenog, Ukr. J. Phys. **55**, 369 (2010).
15. B.E. Grinyuk and I.V. Simenog, Vestn. S.-P. Gos. Univer. Ser. 4, **3**, 116 (2010).
16. D.V. Pyatnytskyi and I.V. Simenog, Yad. Fiz. Energ. **10**, 36 (2009).
17. D.V. Pyatnytskyi and I.V. Simenog, Yad. Fiz. Energ. **11**, 16 (2010).
18. V.I. Kukulín, V.G. Neudachin, Yu.F. Smirnov, EChAYa **10**, 1236 (1979).
19. V.V. Babikov, *Variable-Phase Method in Quantum Mechanics* (Nauka, Moscow, 1976) [in Russian].
20. F. Calogero, *Variable Phase Approach to Potential Scattering* (Academic Press, New York, 1967).
21. S. Ali and A.R. Bodmer, Nucl. Phys. **80**, 99 (1966).
22. S.P. Merkuriev, Yad. Fiz. **19**, 447 (1974).
23. L.D. Faddeev and S.P. Merkuriev, *Quantum Scattering Theory for Several Particle Systems* (Kluwer, Dordrech, 1993).
24. A.I. Akhiezer, A.G. Sitenko, and V.K. Tartakovsky, *Nuclear Electrodynamics* (Springer, Berlin, 1994).
25. R.F. Frosch, J.S. McCarthy, R.E. Rand, and M.R. Yearian, Phys. Rev. **160**, 874 (1967).
26. P.E. Bosted *et al.*, Phys. Rev. Lett. **68**, 3841 (1992).
27. H.De Vries, C.W.De Jager, C.De Vries, At. Data Nucl. Data Tables **36**, 495 (1987).
28. D.R. Tilley, G.H. Kelley, G.L. Godwin *et al.*, Nucl. Phys. A **745**, 155 (2004).

Received 14.02.11

СТРУКТУРНІ ВЛАСТИВОСТІ ЛЕГКИХ КЛАСТЕРНИХ ЯДЕР З ДВОМА ЕКСТРАНУКЛОНИМИ

Б.Є. Гринюк, І.В. Сіменог

Резюме

Досліджено кластерні ядра ${}^6\text{Li}$, ${}^6\text{He}$, ${}^{10}\text{Be}$ та ${}^{10}\text{C}$ як системи, що складаються з α -частинок і двох екстрануклонів. Знайдено структурні функції цих ядер у варіаційному підході. Наведено і пояснено зарядові розподіли густини, формфактори, парні кореляційні функції.